Biomaterials Science

ROYAL SOCIETY OF CHEMISTRY

PAPER

View Article Online
View Journal | View Issue



Cite this: *Biomater. Sci.*, 2022, **10**, 1936



# Tailored therapeutic release from polycaprolactone-silica hybrids for the treatment of osteomyelitis: antibiotic rifampicin and osteogenic silicates†

Lukas Gritsch, *[a] Henri Granel,[b] Nicolas Charbonnel,[c] Edouard Jallot,[a] Yohann Wittrant, [b] Christiane Forestier[c] and Jonathan Lao[a]

The treatment of osteomyelitis, a destructive inflammatory process caused by bacterial infections to bone tissue, is one of the most critical challenges of orthopedics and bone regenerative medicine. The standard treatment consists of intense antibiotic therapies combined with tissue surgical debridement and the application of a bone defect filler material. Unfortunately, commercially available candidates, such as gentamicin-impregnated polymethylmethacrylate cements, possess very poor pharmacokinetics (*i.e.*, 24 hours burst release) and little to no regenerative potential. Fostered by the intrinsic limitations associated with conventional treatments, alternative osteostimulative biomaterials with local drug delivery have recently started to emerge. In this study, we propose the use of a polycaprolactone-silica sol–gel hybrid material as carrier for the delivery of rifampicin, an RNA-polymerase blocker often used to treat bone infections, and of osteostimulative silicate ions. The release of therapeutic agents from the material is dual, offering two separate and simultaneous effects, and decoupled, meaning that the kinetics of rifampicin and silicate releases are independent from each other. A series of hybrid formulations with increasing amounts of rifampicin was prepared. The antibiotic loading efficacy, as well as the release profiles of rifampicin and silicates were measured. The characterization of cell viability and differentiation of rat primary osteoblasts and antibacterial performance were also performed. Gram-positive *Staphylococcus aureus* and Gram-negative *Pseudomonas aeruginosa* and *Escherichia coli* were selected due to their high occurrence in bone infections. Results confirmed that rifampicin can be successfully loaded within the hybrids without significant degradation and that it is possible to tailor the antibiotic release according to need. Once in a physiological environment, the rapid release of silicates was associated with optimal cell proliferation and the overexpression of osteoblastic differentiation. Simultaneously, rifampicin is delivered over the course of several weeks with significant inhibition of all tested strains. In particular, the materials caused a growth reduction of 7–10 orders of magnitude in *Staphylococcus aureus*, the major strain responsible for osteomyelitis worldwide. Our data strongly suggest that PCL/silica hybrids are a very promising candidate to develop bone fillers with superior biological performance compared to currently available options. Thanks to their unique synthesis route and their dual tailored release they can promote bone regeneration while reducing the risk of infection for several weeks upon implantation.

Received 30th December 2021,
Accepted 24th February 2022

DOI: 10.1039/d1bm02015c

rsc.li/biomaterials-science

## 1 Introduction

Osteomyelitis is among the most complex conditions encountered in orthopedic surgery and bone reconstruction. It is defined as a bone tissue destructive inflammatory process caused by a bacterial infection. It can be acute, characterized by soft tissue edema, pus formation and locally decreased blood supply, or chronic, with formation of areas of bone necrosis (*sequestra*) that increase infection recurrence.[1,2] Gram-positive strains are most commonly involved, with a significant predominance of *Staphylococcus* and *Streptococcus* genera. In particular, several reports identified *Staphylococcus*

[a]*Laboratoire de Physique de Clermont, UMR CNRS 6533, Université Clermont Auvergne, 4 avenue Blaise Pascal, 63178 Aubière, France. E-mail: lukas.gritsch@clermont.in2p3.fr*
[b]*Unité de Nutrition Humaine UMR 1019 INRAE, Université Clermont Auvergne, 28 place Henri-Dunant, 63001 Clermont-Ferrand, France*
[c]*Université Clermont Auvergne, CNRS, LMGE, 63000 Clermont–Ferrand, France*

†Electronic supplementary information (ESI) available. See DOI: 10.1039/d1bm02015c

*aureus* as the major responsible worldwide, appearing in 50–70% of tested clinical isolates.[3–5] Several mechanisms can lead to the onset of an infection, including hematogenous, post-traumatic, local spread from contiguous outbreak, *peri*-operative colonization and prosthesis/implant contamination (*e.g.*, periprosthetic joint infection, PJI).[6] Treatment includes a combination of tissue debridement, intense local antibiotic therapies[7–9] and the implantation of a suitable graft when necessary.[1,6] The long-term outcome of the procedure can be very challenging. In particular, the optimization of debridement is considered to be the cornerstone of a successful treatment: since pathological tissues are poorly vascularized, their thorough removal is of chief importance for the antibiotics to be effective and to reduce bone ischemia.[6] However, high debridement means high invasiveness and possibly longer prognosis. Reducing it could preserve the structural integrity of bone, but at the cost of increasing the risk of recurrence.[1,10] In any case, even with optimized debridement, the treatment of osteomyelitis frequently results in significant bone defects that need tailored medical care.[6] In addition, infection sites are typically rich in cytokines (*e.g.*, tumor necrosis factor or interleukin-1). These biomolecules are strong osteolytic promoters and can hinder bone healing, even following a successful intervention.[11,12]

The close relationship between osteomyelitis and bone defects is a strong drive for the development of novel approaches and materials designed to improve bone healing and reduce the risk of infection relapse. A properly engineered biomaterial should not only fill the bone defect but also improve regeneration and fend off possible threats. In other words, it should be both antibacterial and osteostimulative. Driven by the promise of better bone reconstruction, research in the field is investigating many candidate approaches, including drug-loaded synthetic polymers (*e.g.*, polylactic acid, polyglycolic acid),[13–15] composites[16–18] and hydroxyapatites, silver-based nanotechnologies, quaternary chitosan and therapeutic ion releasing bioactive glasses.[19,20] However, despite their promising results in the laboratory, most of these technologies still lack significant clinical data to confirm their efficacy. To date, no commercial product has been successfully launched yet.[21] Currently, the gold standard for bone defect management is the use of gentamicin-impregnated polymethylmethacrylate (PMMA) cements.[22] This technology, however, has several drawbacks, including: (i) the non-degradability and possible toxicity of PMMA, (ii) the thermal degradation of gentamicin during cement setting and (iii) its inadequately fast pharmacokinetics (*i.e.*, burst release of 80–90% of the drug within 5 minutes).[1,3,21] Better results in terms of drug delivery were recently obtained using bioresorbable calcium sulphate bone cements (CSCs) as carriers, giving rise to new alternative possibilities in the treatment of osteomyelitis.[22,23] Gentamicin, vancomycin and tobramycin are the main antibiotics successfully used in conjunction with CSCs.[24] Although desirable, however, the high reactivity and rapid bioresorbability of CSCs is also a key limitation. The resorption rate is too high to grant sufficient bone healing and CSCs are quickly hydrolyzed in the body (in 6 to 12 weeks).[24] In addition, the fast resorption of CSCs was associated with wound serous exudate.[25] Their mechanical properties are also quite poor,[1] offering very limited structural support to the tissue. Generally speaking, both PMMA and CSC offer a sufficient performance to tackle the problem, but also significant drawbacks. They have poor pharmacokinetics and a very low regeneration potential. Furthermore, they are mostly used in conjunction with very common, broad-spectrum antibiotics (*e.g.*, gentamicin). The clinical need for new materials against osteomyelitis remains therefore a pressing issue, with orthopedic surgeons still having few options available whenever looking for antibacterial and osteostimulative bone fillers.[19]

In previous studies, class I polycaprolactone/bioactive glass (PCL/BG) hybrids were successfully synthesized and characterized to be applied for the regeneration of bone defects.[26,27] Organic/inorganic (O/I) hybrids are a family of single-phase materials formed by a network of organic and inorganic moieties combined at the molecular level.[28] They are synthesized using sol–gel chemistry and are organized in five classes.[29] The first two classes of hybrids are both prepared by adding a polymer to a sol–gel synthesis. Class I is characterized by weak O/I intermolecular interactions (molecular entanglement, hydrogen bonding and/or van der Waals forces), while class II presents O/I covalent bonds. Class III and IV are hybrids characterized by the simultaneous polymerization (one-pot synthesis) of both the organic and inorganic components. If O/I interactions are weak, the hybrid is class III, if the organic and inorganic chains are covalently bonded, class IV. Finally, class V are a variation of class III with a single silicate precursor able to liberate organic monomers that can then polymerize.

Our findings confirmed that class I PCL/BG hybrids have strong osteostimulative potential *in vitro*, showing enhanced apatite formation, promotion of cell proliferation and of osteoblastic differentiation.[26] These results were corroborated *in vivo* in a mouse calvaria model, where tissue ingrowth was significantly increased compared to a commercial benchmark.[27] Sol–gel silicates were also found to be particularly effective in the incorporation of antibiotics and their subsequent controlled release, thanks to templating effects occurring during synthesis.[30] In light of these promising findings, the aim of this work was to engineer a material with the beneficial properties of PCL-based hybrids in terms of bone regeneration and simultaneous antibacterial effect: a platform technology with a dual (*i.e.*, with two therapeutic effects) and decoupled (*i.e.*, with independent kinetics) controlled release of therapeutic silicates and an osteomyelitis-specific antibiotic, rifampicin. Rifampicin is an RNA synthesis blocker very effective in the treatment of staphylococcal infections, especially when delivered locally.[7] PCL/silica hybrids were chosen as candidate for the design and development of antibiotic bone fillers with superior performance both in terms of sustained release of the drug and regenerative potential when compared to current competitors (*e.g.*, PMMA, CSC). To reach

the purpose, the hybrid synthesis protocol was adapted to allow the incorporation of rifampicin without significant degradation of the antibiotic. Preliminary dilution assays were performed to identify the cytocompatibility concentration range and minimal inhibitory concentration of the antibiotic for the tested bacterial strains. In parallel, an array of rifampicin-loaded PCL/silica hybrids with several drug loadings was successfully prepared and physicochemically characterized. In particular, the release of therapeutic agents from the materials, namely silicates and rifampicin, was measured to match the desired beneficial concentrations of both. Finally, a biological characterization was carried out in order to confirm the efficacy of the hybrids in terms of osteostimulation (on rat primary osteoblasts) and antibacterial effect (against *Staphylococcus aureus*, *Escherichia coli* and *Pseudomonas aeruginosa*).

# 2 Experimental section

## 2.1 Identification of a rifampicin concentration range of interest

**2.1.1 Rifampicin minimum inhibitory concentration.** A set of preliminary dilution assays was initially performed in order to determine the minimum inhibitory concentration (MIC) of rifampicin and identify the region of interest of concentration for this study. Three relevant bacterial strains were considered: *Staphylococcus aureus* (clinical isolate from osteoarticular infection, previously fully characterized elsewhere[31–33]), *Pseudomonas aeruginosa* (ATC 27853) and *Escherichia coli* (ATCC 25922). Isolated colonies of each strain were cultured overnight in nutrient broth (LB broth Lennox, CONDA) at 37 °C under agitation (100 rpm), resulting in bacteria suspensions of $\sim 10^9$ CFU mL$^{-1}$ the following day. The suspensions were diluted to $10^6$ CFU mL$^{-1}$ by adjusting their optical density at 600 nm (Genesys™ 30 spectrophotometer, Thermo Fisher Scientific). The final inoculum was mixed with an array of subsequent dilutions of rifampicin in alpha Minimum Essential Medium (αMEM, Gibco) ranging from 0 to 200 μg mL$^{-1}$. At four concentrations (0, 1, 10 and 50 μg mL$^{-1}$), a standard Gram staining (gentian violet/fuchsin) was also performed to characterize the strains and identify possible changes in cell shape following the exposure to rifampicin. Stained colonies were spread onto glass slides and observed using a Leica DM1000 optical microscope combined with a Leica DFC295 digital camera and the Leica Application Suite Version 3.8.0 software.

**2.1.2 Rifampicin cytocompatibility range.** Rat primary osteoblasts (RPOs) were isolated from the enzymatic digestion of fetal Wistar rat calvaria explants following a previously described method.[34] In short, bone pieces were incubated for 15 minutes in a solution of penicillin/streptomycin (p/s, 1%), collagenase IA (0.1%), and dispase II (0.2%) in cell culture αMEM. The process was carried out at 37 °C and repeated four times. The obtained RPOs were then plated at 10 000 cells per cm$^2$ and cultured (37 °C, 90% humidity and 5% $CO_2$) in αMEM supplemented with 10% fetal bovine serum (FBS) and 1% p/s until confluence. Finally, the cells were collected and frozen in αMEM with 20% FBS and 7% dimethyl sulfoxide (DMSO) until the time of testing. To obtain a first set of information regarding the interaction between rifampicin and RPOs the cells were cultured in presence of the antibiotic. RPOs were seeded in 24-well plates at a density of 20 000 cells per well (as per supplier guidelines) and cultured for one week using αMEM with 10% FBS, 1% p/s and various concentrations of rifampicin ranging from 0 to 100 μg mL$^{-1}$. At two time points (2 and 7 days) the cell viability was measured using XTT Viability/Proliferation Kit II (Sigma-Aldrich), a colorimetric tetrazolium-based assay that correlates the viability of cells with the absorbance at 550 nm. The test was performed according to the protocol provided by the supplier.

## 2.2 Synthesis of PCL/silica hybrids with and without rifampicin

Polycaprolactone/silica hybrids with a 70 : 30 organic-to-inorganic ratio were synthesized by sol–gel chemistry from tetraethyl orthosilicate (TEOS) (99% purity, Sigma-Aldrich). TEOS was initially dispersed in absolute ethanol (Sigma-Aldrich) and hydrolyzed for 30 minutes adding 2 M HCl (diluted from 37% fuming HCl, Sigma-Aldrich). The molar ratio between the components was ethanol : $H_2O$ : TEOS : HCl = 3.7 : 2 : 1 : 0.07, according to a previously optimized protocol.[26] In parallel, polycaprolactone (PCL, $M_n$ = 80 kDa, Sigma-Aldrich) was dissolved in tetrahydrofuran (THF) at a concentration of 20% w/v. Once the polymer is completely dissolved, rifampicin (≥97%, suitable for cell culture, Sigma-Aldrich) can be incorporated into the hybrid: three different quantities of antibiotic (see Table 1) were first dissolved into a negligible volume of solvent and then added to the PCL solution. Control samples (PS) were synthesized omitting this step.

After the hydrolysis of TEOS, a saturated solution of NaOH (Sigma-Aldrich) in ethanol was prepared, filtered (0.2 μm PVDF syringe filter, Thermo Scientific) and added dropwise to the TEOS solution until the pH, initially very low (*i.e.* <0), is adjusted to 5. This increase allows for the condensation of the silicate precursor in the sol, ultimately leading to its gelation, while also protecting the antibiotic from degradation. Right before complete gelation, the PCL and TEOS solutions are mechanically mixed and sonicated for 1 hour to obtain a homogeneous hybrid sol. The sol is aged for 24 hours before letting the solvent evaporate, obtaining hybrid films. The films

Table 1 Summary of the organic/inorganic (O/I) ratio and the rifampicin content of the four formulations of hybrid synthesized in this study

| Formulation | Rifampicin per gram of material (mg) | Theoretical PCL : $SiO_2$ : rifampicin weight ratio |
|---|---|---|
| PS | 0 | 70 : 30 : 0 |
| PSRL | 0.36 | 69.993 : 30 : 0.007 |
| PSRM | 3.6 | 69.93 : 30 : 0.07 |
| PSRH | 18 | 69.7 : 30 : 0.3 |

were grinded and compressed into standard 100 mg pellets (Ø = 13 mm) used in all characterizations.

### 2.3 Physicochemical characterization

**2.3.1 Stability in simulated physiological conditions.** The stability of hybrids in a biological environment was tested *in vitro* by monitoring weight loss and pH variation over a period of 14 days in αMEM. Samples ($n$ = 5) were immersed in the medium and incubated at 37 °C for two weeks. The medium was refreshed every two days. Both pH and sample weight were measured at several time points (1, 3, 7 hours and 1, 3, 5, 7, 10, 14 days). The 2-week time window was chosen to monitor variations in material stability simultaneous to cell growth. Longer timepoints were not considered since polycaprolactone and crosslinked silica have relatively slow degradation rates *in vivo* (*i.e.*, years). It is therefore safe to assume that no significant phenomenon linked to massive degradation is expected to occur within the first month.

**2.3.2 Contact angle.** The surface wettability of PCL/silica hybrids with and without rifampicin was also investigated to identify possible variations in hydrophilicity following the addition of the antibiotic. Static contact angle measurements were performed at room temperature using a simple custom set-up consisting of a manually adjustable base and a microliter syringe (25 μL Model 702 N, cemented 2 inch needle, 22s gauge, point style 2, Hamilton Company). A 10 μL droplet was initially deposited on the sample. Then, after a one-minute lag to reduce the impact of absorption on the results, images of the contact angle were acquired using an industrial camera UI-3370CP Rev.2 (4 MP CMOS sensor CMV4000) equipped with a Sigma 105 mm f/2.8 macro lens (Imaging Development Systems, IDS). Three independent measurements per sample type were performed, with two angles (left and right) per measurement. Contact angle calculation was carried out using ImageJ (NIH, USA) with prior image elaboration on GIMP (thresholding, brightness/contract correction, color inversion).

**2.3.3 Fourier-transform infrared spectroscopy.** Fourier-transform infrared spectroscopy (FTIR) was used to characterize the chemical nature of the materials. The acquisition of infrared spectra of all samples was carried out using a Nicolet 380 FT-IR (Thermo Fisher Scientific) equipped with a diamond Attenuated Total Reflectance (ATR) accessory. Data (32 scans, resolution of 4 $cm^{-1}$) were collected in the mid-IR region (4000–400 $cm^{-1}$) in triplicates and from different regions of each sample.

### 2.4 Controlled release of ions and antibiotic

**2.4.1 Extraction of loaded rifampicin.** To estimate the efficacy of our synthesis route, a protocol of extraction and quantification of the rifampicin loaded in the hybrids was developed. The results were compared to the theoretical drug concentration per formulation (as per Table 1). To retrieve the antibiotic loaded into the materials, 100 mg of all hybrid formulations were left to dissolve in 10 mL of THF for 2 days. Two cycles of sonication were also performed, at 24 and 48 hours, respectively. This results in the formation of a suspension of inorganic silicate nanoparticles (insoluble in the solvent) dispersed in a PCL and rifampicin solution in THF. The suspensions were centrifuged for 1 minute at 2000 g, then the surnatant was collected and stored for further analysis.

**2.4.2 Rifampicin release.** The release of antibiotic was characterized in colorless αMEM. The lack of phenol red (pH indicator) avoids possible alterations of the spectra. Rifampicin-loaded hybrids were immersed in the medium and incubated in an orbital shaker at 37 °C and 250 rpm. At selected time-points (1, 3, 5, 7, 10 and 14 days) the medium was retrieved and tested to quantify its concentration in antibiotic.

**2.4.3 First derivative UV-Vis spectrophotometry.** A spectrophotometric method developed by Walash *et al.*[35] was used to quantify rifampicin in both the solutions retrieved from hybrids (loading efficacy) and in released products in αMEM. The method and its validation are described in detail elsewhere.[35] Briefly, at every experiment, a calibration curve was prepared using known concentrations of rifampicin in a relevant solvent (αMEM or THF, depending on the experiment). The first derivative curves of the spectra of solutions were recorded in 1 cm quartz cells over the range of 800 to 200 nm using a Cary 50 UV-Vis spectrophotometer (Varian, USA) at 4800 nm $min^{-1}$ scan rate. According to the method, the amount of rifampicin is proportional to the value of the first derivative of the absorbance at 500 nm.

**2.4.3 Quantification of silicon release by ICP-OES.** The release of silicon ions (in the form of various silicates, such as silicic acid) was performed in αMEM and measured by Inductively Coupled Plasma Optical Emission Spectrometry (ICP-OES). Standard hybrid pellets of all formulations were immersed in culture medium at a 20 mg $mL^{-1}$ ratio and put in an orbital shaker at 37 °C and 250 rpm. At given time-points the medium was retrieved and the concentration of Si ions was determined by ICP-OES (Ultima C, HORIBA Jobin Yvon). It is known from previous studies that the release profile of this type of hybrids is relatively steep (*i.e.*, it reaches plateau within the first few days). Therefore, the chosen time-points were 30 minutes, 1, 3, 5, 7 hours and 1, 2, 3 days.

### 2.6 Microbiology

**2.6.1 Agar disk diffusion test.** A first estimation of the antibacterial properties of rifampicin-loaded hybrids was obtained by an agar disk diffusion assay (halo test). Bacteria populations of *S. aureus* (clinical isolate), *P. aeruginosa* (ATC 27853) and *E. Coli* (ATCC 25922) in LB broth were prepared as described in section 2.1.2 and then diluted down to a density of *circa* $10^7$ CFU $mL^{-1}$. This value is high enough to grant the development of an even layer of colonies on the agar plate. The adjusted inoculum was deposited and spread homogeneously onto a Petri dish (Ø = 94 mm) filled with Agar LB Miller (CONDA). A sample per formulation was then set on top of the agar and the dish was incubated for 24 h at 37 °C and high relative humidity (80%). The width of the inhibition annulus was then calculated as the difference between external radius and internal radius (*i.e.*, 7.5 mm).

**2.6.3 Colony forming units counting and antifouling test.** Quantitative evaluation of the antibacterial effect of rifampicin-loaded hybrids was also carried out by colony forming units (CFUs) counting using the same strains as above. Suspensions of the three bacteria in αMEM (density = $10^6$ CFU $mL^{-1}$) were incubated for 24 hours in presence of pellets of all the synthesized formulations. The same medium used for eukaryotic cells was chosen for better comparison between the results of microbiology and the ones obtained when studying RPOs. At given time-points (3, 6 and 24 hours) each suspension was retrieved, diluted according to need and plated on LB agar Petri dishes using an automatic diluter and plater (easySpiral Dilute, Interscience). In parallel, the number of bacteria adhering on the pellets was also measured to estimate possible antifouling properties of the materials. Pellets were rinsed three times in saline ($\varphi$), then immersed in 5 mL of $\varphi$ and sonicated for 10 minutes to detach cells from the surface. Afterwards pellets were disposed of and the remaining bacterial suspension in $\varphi$ was diluted when necessary and plated on agar. After further 24 hours of incubation, colonies were counted using an automatic colony counter (Scan 300, Interscience).

### 2.7 Osteoblast response

**2.7.1 Cytotoxicity and cell viability.** In parallel with bacterial cultures, RPOs were cultured in presence of the dissolution products of antibiotic-loaded hybrids to evaluate possible cytotoxicity and characterize their influence on cell viability and proliferation. RPOs were seeded at a density of 20 000 cells per well and cultured for one week using eluates of the materials in αMEM (with 10% FBS and 1% p/s). As described in section 2.1.1, cell viability was assessed at 2 and 7 days using the XTT Viability/Proliferation Kit II (Sigma-Aldrich), which correlates viability with the respective value of absorbance at 550 nm.

**2.7.2 Cell adhesion and morphology.** Cells were also cultured directly on the hybrid samples in order to observe cell morphology and investigate possible changes in adhesion. RPOs were seeded on the surface of PSRM pellets and cultured in αMEM overnight. On the second day, the samples were fixed using 1.6% glutaraldehyde in 0.2 M sodium cacodylate buffer (pH 7.4). They were stored in the fixative for 4 days at 4 °C. Subsequently, they were washed three times with a sodium cacodylate buffer and post-fixed 1 hour with 1% osmium tetroxide. After an additional wash in distilled water, samples were dehydrated by graded ethanol, treated with hexamethyldisilazane (HMDS) and dried overnight. Scanning electron microscopy (SEM) was performed upon sputter coating with carbon (Emitech E6500, Quorum) using a Regulus 8230 (Hitachi) at 2 kV.

**2.7.3 ALP activity.** A preliminary investigation of the osteostimulative effect of silicates release from the hybrids was performed by measuring variations in the activity of enzymatic alkaline phosphatase (ALP) at 14 days of culture. RPOs were cultured as described in previous sections. At the desired time-point, culture wells were washed three times in PBS and treated with NP40 lysis buffer. Resulting cell lysates were incubated in a solution of 40 mM *p*-nitrophenyl phosphate (Sigma-Aldrich) and alkaline assay buffer (Abcam). The production of *p*-nitrophenol as a function of the ALP activity was determined by spectrophotometric measurement at 405 nm and at 37 °C. The absorbance was expressed as the mean value per minutes. Results were normalized with respect to the total amount of proteins in the respective sample as obtained by a bicinchoninic acid (BCA) assay.

### 2.8 Statistical analysis

Results of each population were given as mean ± standard deviation (SD). Comparisons to highlight statistically significant differences were performed by one-way analysis of variance (ANOVA) with a significance of $\alpha = 0.05$ (OriginLab 8.5 data analysis software).

## 3 Results and discussion

### 3.1 Rifampicin tailoring

Prior to materials preparation, the effect of rifampicin on target cells, both eukaryotic and prokaryotic, was characterized. This step supports the design of the controlled release platform, providing valuable information on the effective concentration ranges to inhibit bacteria without exerting major detrimental effects on osteoblasts. Observations after Gram staining indicated that samples exposed to rifampicin show a significantly lower number of bacteria, often tending to zero. An interesting morphological phenomenon associated with high concentrations of rifampicin was also assessed with the two Gram-negative bacilli: cells appear smaller and with a round shape (Fig. 1, panels B1 and C1). Rifampicin is known to significantly alter the attachment points of the nucleoid to the cell membrane in *E. coli.*[36] However, to date we found no information on possible effects of the drug on the overall cell morphology and these changes are likely due to a global reaction to the stress induced by the antibiotic. In addition, no such variation was detected for *S. aureus*, possibly as a consequence of its higher susceptibility to rifampicin, which impedes the onset of reactive mechanisms by the cells.

Levels of MIC can vary according to strains,[37] bacterial genomic variations (*i.e.*, resistance development)[38] and culture and testing conditions.[39] These variations can often be significant, up to three or four orders of magnitude. In this study, the dilution assays performed with the three bacterial strains of interest in the context of osteomyelitis allowed the determination of the MIC of rifampicin against *S. aureus*, *P. aeruginosa* and *E. coli* at 0.05 μg $mL^{-1}$, 50 μg $mL^{-1}$ and 25 μg $mL^{-1}$, respectively (Fig. 2).

Regardless of the strain, MIC values measured in this study were generally consistent with current results found in literature. The clinical strain of *S. aureus* tested in this study was found to be highly susceptible to rifampicin. Relatively higher values were obtained with the two Gram-negative strains. This

 

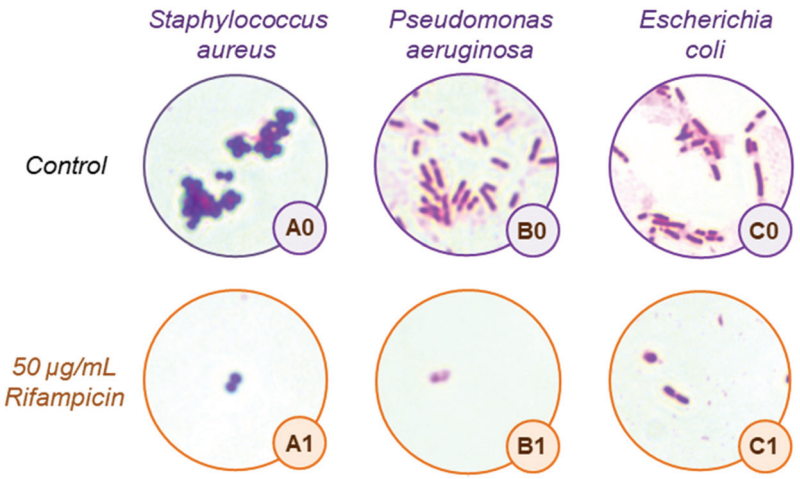


**Fig. 1** Gram staining of the three bacteria used in this study cultured in standard conditions (top, A0 to C0) and in presence of a rifampicin concentration of 50 µg $mL^{-1}$ (bottom, A1 to C1). Pictures were obtained by optical microscopy (100× magnification).

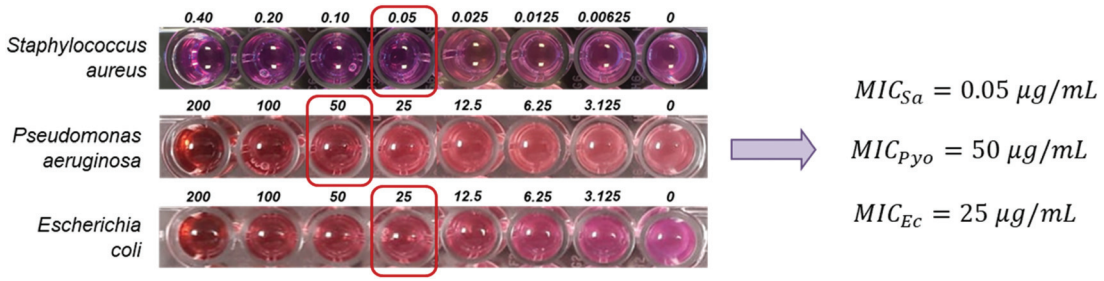


**Fig. 2** Rifampicin dilution arrays used to identify the MICs of the strains *S. aureus* (Sa), *P. aeruginosa* (Pyo) and *E. coli* (Ec). Each MIC corresponds to the lowest concentration leading to a clear (*i.e.*, not turbid) suspension. The values are highlighted and reported on the right.

is not surprising, since these bacilli are generally known for their lower susceptibility to the molecule.[40]

A similar approach was adopted for the determination of RPOs behavior in presence of rifampicin. Cell viability was measured using XTT at 2 and 7 days of incubation. The results of the test are reported in Fig. 3.

A decrease in viability can be observed already at 2 days, starting above 10 µg $mL^{-1}$ and increasing dose-dependently. Up to 70 µg $mL^{-1}$, the reduction is limited, with viability sitting around 70–80% of the control. However, 100 µg $mL^{-1}$ of rifampicin were found to halve the viability already at 2 days. The results were confirmed by examining the viability RPOs after one week of culture: a significant decrease to 70% of the control was measured already for cells exposed to 10 µg $mL^{-1}$ of rifampicin. At 50 µg $mL^{-1}$ the values are as low as 40%, decreasing to almost no viability at 100 µg $mL^{-1}$. Similar results were obtained by Winters *et al.*,[41] who confirmed the absence of specific cytotoxic effects of rifampicin on human cells up to 20 µg $mL^{-1}$. Differently, studies of the effect of rifampicin showed no cytotoxic effect up to 85 µg $mL^{-1}$ when using a hepatic cell line (HepG2).[42] Probably due to the more sensitive nature of primary cells compared to cell lines, our data suggest that high concentrations of rifampicin have a sig-

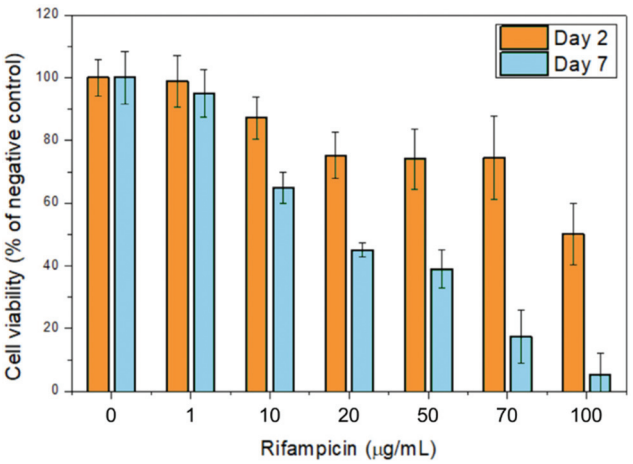


**Fig. 3** Cell viability of rat primary osteoblasts (RPOs) at 2 and 7 days as a function of rifampicin concentration (0–100 µg $mL^{-1}$). Data at each day are normalized with respect to the viability of the respective negative control. The progressive inhibition of RPOs and the cytotoxic effect at higher concentrations (>10 µg $mL^{-1}$) can be clearly observed.

nificant cytotoxic effect. For this reason, in view of the design of the hybrid materials, the release concentration was tailored in the 0 to 20 μg $mL^{-1}$ range.

### 3.2 Sol–gel synthesis, rifampicin loading efficacy and *in vitro* degradation behavior

Homogeneous PCL/Silica hybrids with and without rifampicin were successfully synthesized (Fig. 4). In particular, the process appears reproducible, resulting in materials with antibiotic evenly distributed within the network.

Burning out the organic component of the hybrids at high temperature also confirmed that the organic-to-inorganic ratio is in accordance with its theoretical value of 70 : 30, only slightly lower (Table 2). The difference is probably due to a partial burn-out of low molecular weight inorganic residues.

Although a key topic surrounding the synthesis of organic/inorganic hybrids is the incorporation of calcium ions for increased apatite forming ability,[28,43] in this study materials with pure silica as inorganic component were prepared. In early trials (data not shown), we observed the occurrence of a very rapid and significant degradation of rifampicin in presence of either high pH or calcium ions. This characteristic of the drug makes it incompatible with previously adopted synthesis protocols used for the preparation of binary Si–Ca hybrids. Therefore, in this study calcium was removed and a minimum amount of sodium was used to adjust the pH of the solution pot to a value that maximizes rifampicin stability (*i.e.*, pH ∼ 5). The spectrophotometric results on loading efficacy confirmed that this technique did not significantly degrade rifampicin. The right columns of Table 2 show the measured and theoretical content of rifampicin loaded in each pellet sample (100 mg) depending on the hybrid formulation. Little to no variation between the two values was observed for every tested material. Note that for PSRL the standard deviation is relatively high since the amount of rifampicin loaded is minimal and rather close to the sensitivity threshold of spectrophotometry. Since the selected spectrophotometric method is specific for rifampicin and not its degradation products,[35] it is safe to assume that loading PCL/silica hybrids with rifampicin does not significantly hinders the structure (and thus the antibacterial effect) of the antibiotic.

**Table 2** Summary of the weight percentages of the inorganic component (theoretical value = 30%), the theoretical loaded rifampicin and the measured antibiotic retrieved from the materials after synthesis (both expressed as mass per 100 mg sample)

| Formulation name | Inorganic fraction (%) | Theoretical loaded rifampicin per sample (μg) | Measured loaded rifampicin per sample (μg) |
|---|---|---|---|
| PS | 27.6 ± 1.3 | 0 | 1 ± 2 |
| PSRL | 26.5 ± 2.1 | 36 | 32 ± 15 |
| PSRM | 27.1 ± 1.6 | 360 | 280 ± 60 |
| PSRH | 25.8 ± 1.9 | 1800 | 1800 ± 100 |

A statistically significant, although minor, effect of rifampicin was observed when studying the wettability of the samples. Contact angle measurements identified two distinct phenomena: (i) an increase in hydrophilicity in PCL/silica hybrids compared to a PCL control and (ii) a less prominent, but nevertheless significant, decrease in contact angle following rifampicin loading. In general, contact angles measurements were in line with values reported in literature for similar materials, both for PCL[44,45] and its hybrids.[26] PCL showed a rather typical mild hydrophobic behavior ($\theta$ = 83° ± 2), reduced after the addition of silica. The incorporation of the inorganic component determines a statistically significant increase in hydrophilicity, expressed as a decrease of *circa* 10° in contact angle. This increase can be beneficial to cell adhesion.[46] While PSRL is comparable with PS, a further decrease of 5–10° compared to the PS control was observed for higher loadings of rifampicin (PSRM and PSRH), indicating that the antibiotic contributes to the overall hydrophilicity of the material despite its

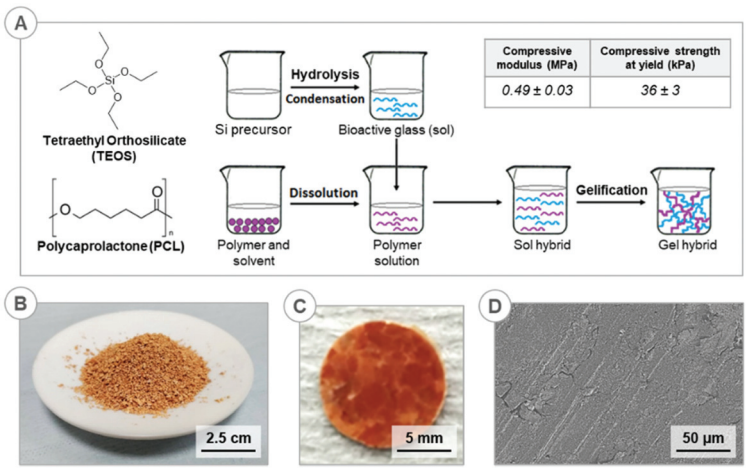


**Fig. 4** Schematic representation of the synthesis procedure (A). The inset shows typical mechanical parameters for this type of hybrid taken from ref. 26. Pictures of the material (PSRM, in this case) are also presented: powder (B) and pellet (C) forms are both shown. An SEM micrograph (D) of the same pellet can be also observed (magnification 300×).

 

modest amount (see Table 1). This is somewhat surprising since rifampicin is generally considered hydrophobic (Fig. 5).[47]

The stability of the hybrids in a suitable medium was then investigated. Rifampicin was found to have negligible effects on the degradation behavior of the materials. As confirmed by monitoring the weight variation in αMEM, no variation was observed following the addition of antibiotic. All samples followed a typical trend already reported for class I polycaprolactone-based hybrids by Bossard *et al.*:[26] an initial loss of soluble inorganic moieties, followed by a higher decrease due to the de-esterification of PCL, reaching a weight loss of 15–20% after 14 days (Fig. 6). The degradation rate significantly differ from the reported value of 13.2% weight loss after 8 weeks.[26] However, previous results were obtained in static conditions, while in the present study semi-dynamic conditions were preferred. It is possible that medium renewal accelerated the degradation of PCL.[48]

In parallel, possible changes in pH were also monitored. Data seem to suggest the occurrence of a minor increase in pH probably associated with the leaching of residues of sodium used during the synthesis. The increase was found to be not statistically significant, indicating that the hybrids do not hinder the buffer capacity of αMEM and thus do not create an alkaline and possibly harmful microenvironment for cells, as it is sometimes the case for bioactive glasses.[49]

Both weight loss and pH measurements confirmed that PCL/silica hybrids are stable in simulated physiological conditions, degrading slowly and evenly, and show low risk of cytotoxicity due to alkalinization of the medium. They can be deemed appropriate carriers for the long-term delivery of rifampicin. In addition, as already suggested by other authors,[26,50] these hybrids offer superior degradation properties compared to other candidate materials for bone grafting and orthopedic applications.

The characterization with ATR-FTIR was used to study the chemical nature of the two phases, organic PCL and inorganic silica, as well as on the interaction between them. In Fig. 7 the FTIR spectra of PCL (as a control) and all formulations are reported.

Typical IR peaks of PCL were observed for all samples.[51–53] In particular, two peaks of the asymmetrical and symmetrical stretching of carbon–hydrogen bonds centered at 2937 and 2860 $cm^{-1}$ ($\nu$C–H), the sharp characteristic peak of PCL due to carbonyl stretching at 1720 $cm^{-1}$ ($\nu$C═O), the peaks of carbon–hydrogen bending between 1471 and 1365 $cm^{-1}$ ($\delta$C–H) and the three peaks of the carbon–oxygen stretching of ester groups ($\nu$C–O) at 1294, 1240, and 1170 $cm^{-1}$. Once silica is introduced into the polymeric matrix, all the peaks typically related to the vibrations of the Si–O–Si cage occur.[54] Particularly evident are the symmetric and asymmetric stretching at 825 $cm^{-1}$ and 1050 $cm^{-1}$ (Fig. 8A), as well as a low wavenumber bending vibration peak (600 $cm^{-1}$).[55–57]

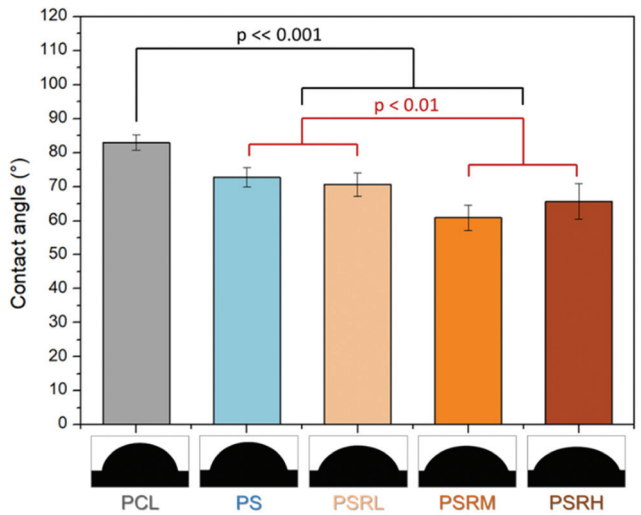


Fig. 5 Droplet profiles and contact angle measurements for all formulations of PCL/silica tested ($n$ = 3). Note the effect of both the introduction of silica gel ($p \ll 0.001$) and of rifampicin ($p < 0.01$) on the hydrophilicity of the samples.

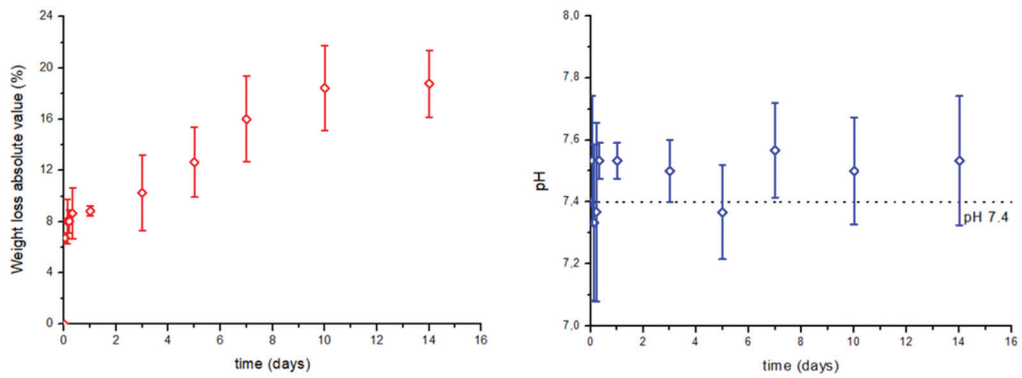


Fig. 6 Graphs showing a typical trend for weight loss (left) and pH (right), following immersion in culture medium for PCL/silica hybrids (results for PSRM are shown, other samples are comparable). The measurements are not affected by the addition of rifampicin: no statistically significant variation was observed varying the concentration of antibiotic ($p > 0.05$, see ESI†).

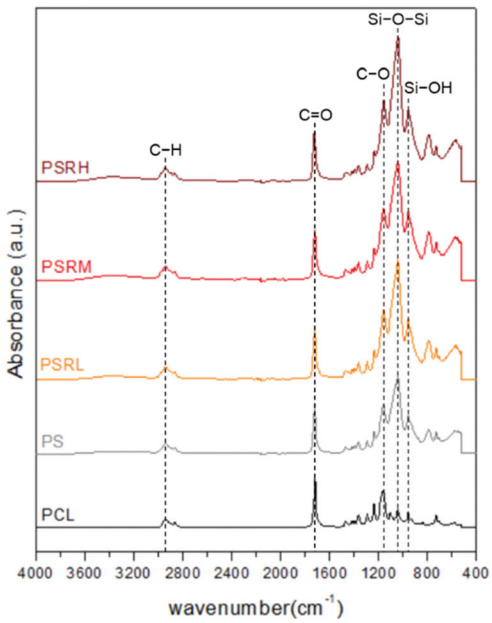


Fig. 7 Comprehensive FTIR spectra (4000–400 $cm^{-1}$) of PCL (bottom) and the four formulations of PCL/silica hybrids tested in our study. The major characteristic peaks of PCL (C–H, C=O, C–O), silica gel (Si–O–Si, Si–OH) and rifampicin (C–H) are highlighted. All spectra are normalized with respect to the characteristic peak of PCL at 1720 $cm^{-1}$.

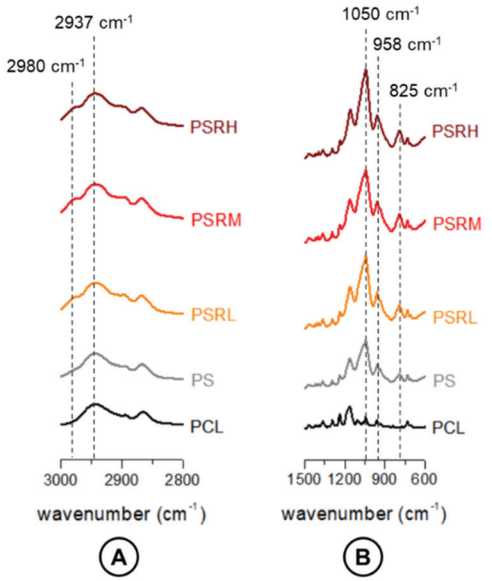


Fig. 8 (A) FTIR spectra highlighting the appearance of a new peak at 2980 $cm^{-1}$ in correspondence of the stretching vibration of C–H following the addition of rifampicin. (B) FTIR spectra comparing the 1500–900 $cm^{-1}$ range before and after sol–gel synthesis. Note the carbon–oxygen ester stretching of PCL at 1170 $cm^{-1}$ and the appearance of peaks associated with silica gel: Si–O–Si (1050 and 825 $cm^{-1}$) and Si–OH (958 $cm^{-1}$).

Interestingly, only minor peaks associated with silanol groups were detected, indicating that the great majority of TEOS reacted during the sol–gel process. This result is unexpected as hybrid systems are usually characterized by significant Si–OH peaks, especially by the hydroxyl vibration of self-associated silanols, centered at 3400 $cm^{-1}$. In addition, silanols are reported to highly change the shape of the characteristic peak of PCL at 1720 $cm^{-1}$ as a consequence of the H-bonds between silanols and the carbonyl groups of PCL.[58] In this study, this peak remains unvaried, regardless of the formulation. These observations led to the conclusion that the preparation of the hybrid sol did not hinder the polycondensation of TEOS, leading to few unreacted silanols and, as a consequence, to little H-bonding between the inorganic and organic component. The interaction between the two components of a hybrid is known to be a major drive for the development of materials with unique properties.[59] For this reason, improving the organic–inorganic interactions in antibiotic-loaded PCL/silica hybrids could offer promising future developments.

The FTIR analysis was also used to confirm the presence of rifampicin in the samples. Unfortunately, when adding rifampicin, only minor variations were observed. This was probably due to the low amount of antibiotic compared to the overall mass of the material and to the overlapping between the characteristic peaks of rifampicin and PCL, especially in the 1000–1500 $cm^{-1}$ range. However, two small differences were observed following antibiotic loading: the occurrence of a new shoulder peak at 2980 $cm^{-1}$ and a significant increase in intensity of the peak at 958 $cm^{-1}$ (Fig. 8B). These variations are consistent with the occurrence of interactions between the rifampicin within the hybrid material and the inorganic component of its carrier matrix.[22] An alternative hypothesis is that the 958 $cm^{-1}$ could be ascribed to minor Si–OH stretching while the shoulder peak to the vibrations of methyl and methylene groups in rifampicin.[60] These results substantiate the successful loading of rifampicin, as previously verified by spectrophotometry. The antibiotic seems well dispersed inside the material and interacting with both the organic (PCL) and inorganic (silica) components of the single-phase hybrid. However, due to signal weakness, the results in this respect cannot be deemed conclusive. Therefore, infrared spectroscopy should be avoided when investigating the rifampicin content in PCL/silica hybrids.

### 3.3 Dual and decoupled release of therapeutic agents

Rifampicin-loaded PCL/silica hybrids are characterized by the ability of simultaneously releasing therapeutic agents with potential beneficial effects on the proliferation of osteoblasts and the inhibition of bacterial growth (*i.e.*, dual release). In addition, owing to the different chemical relation between the therapeutic agents and the matrix, the dual release is expected to follow independent release kinetics for silicates and rifampicin (*i.e.*, decoupled release). Before testing the biological performance of the materials, the release of therapeutics was evaluated immersing samples in αMEM. Silicates release from the inorganic component of the hybrids was measured by ICP-OES (Fig. 9). Results indicate that the concentration of Si ions in the medium quickly increases, reaching a plateau of saturation

 

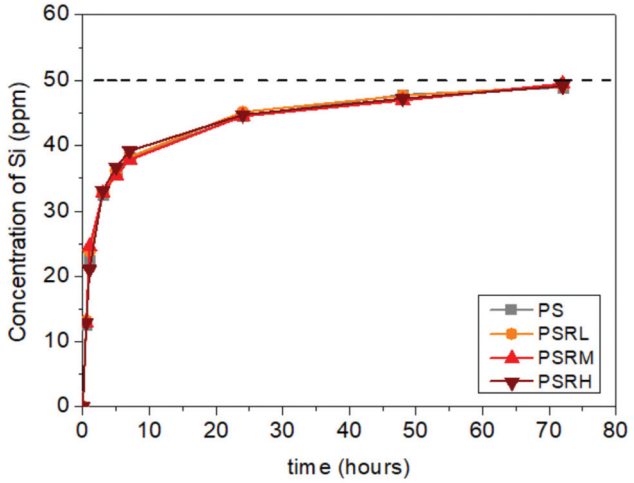


Fig. 9 Silicon release from PCL/silica hybrids immersed in αMEM. As expected, concentrations measured by ICP-OES do not vary depending on the rifampicin content.

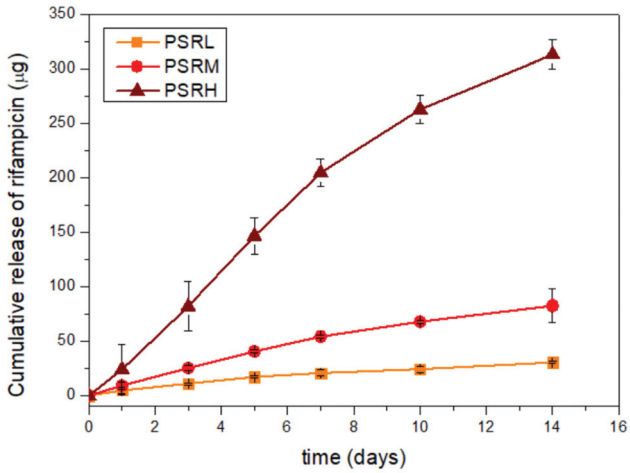


Fig. 10 Cumulative release of rifampicin from all the formulations of tested samples. The antibiotic content in the medium is dependent on the loaded amount, confirming that this technology can be used to tailor rifampicin release.

of *circa* 50 ppm after the first day of immersion. This release is due to the dispersion in water of unreacted reagents and silicate oligomers liberated from the hybrid matrix. As expected, no variation associated with rifampicin loading was observed, given that the organic-to-inorganic ratio remained unvaried across all formulations. The rapid silicon burst release in simulated body fluids is a well-documented phenomenon for similar hybrid materials[26,27] and silica-based sol–gel glasses.[61,62] If medium is replenished, the burst repeats with similar kinetics, presenting a steady concentration of silicates in aqueous environment, up to the solubility limit of silica in water (~50 ppm). These silicates are known to have osteogenic effects on eukaryotic cells, including promotion of osteoblastic differentiation, bone mineralization and secretion of extracellular matrix (ECM).[63] Our results corroborate the hypothesis that PCL/silica hybrids could offer a beneficial sustained release of silicates, supporting cells during the first phases of adhesion and differentiation.

The release of rifampicin was measured calculating the first derivative of the absorbance at 550 nm, which was previously confirmed to be specific for the quantification of the antibiotic.[35] Direct UV-Vis determination of rifampicin can also be performed by measuring the peaks at 330 and 475 nm. However, the derivative technique is more robust and accurate. In particular, it can detect the drug even in presence of its degradation products (mainly 3-formyl rifampin and rifampin quinone), expected to be present as a consequence of sol–gel synthesis. The spectrophotometric results showed that a remarkable almost linear trend of release over 14 days of immersion in medium (Fig. 10). This confirms that PCL/silica hybrids can be considered as an ideal candidate when it comes to delivering a sufficient quantity of rifampicin over a long period of time without harmful burst release. Upon contact with an aqueous medium (in this study αMEM), rifampicin gets progressively released from the matrix *via* diffusion thanks to the concentration gradient between the material and the surrounding environment. This property could effectively protect from infections even several weeks after implantation. For instance, after 14 days of immersion, 30.7 μg, 82.8 μg and 313.5 μg of rifampicin were released by PSRL, PSRM and PSRH, respectively. These quantities account for the 85%, 23% and 17% of the total antibiotic loaded in each formulation. The quantification shows that the released amount of rifampicin depends on the quantity initially added to the materials, confirming that the delivery of antibiotic can be controlled by tailoring its loading.

The performance of our candidates was also satisfactory when compared to previously reported approaches for the local delivery of rifampicin. Polymer-based technologies are generally characterized by a rapid burst. For instance, drug release was reported to reach 100% within the first day using either polyhydroxybutyrate microsphere[64] or chitosan gels.[65] Better results could be obtained using inorganic strategies, probably thanks to the interaction between the inorganic matrix and the drug.[22] For instance, investigations into a biphasic bone cement material composed of calcium sulphate ($CaSO_4$) and nano-hydroxyapatite reported a similar sustained release trend, slowly ramping to 25–30% of released rifampicin after 2 weeks of immersion.[22] The use of hybrids as carriers could offer an additional improvement over $CaSO_4$-based cements owing to their superior mechanical and degradative properties.[66] In addition, class I PCL hybrids already have a promising history of *in vivo* regeneration potential compared to more inert candidates currently in use.[27]

When it comes to surgical site infections, the initial stages after implantation are often the most critical. The release after 24 hours should be assessed to gain more insight into the potential of the materials. PSRL, PSRM and PSRH delivered

4.9 μg, 9.3 μg and 24.1 μg of antibiotic, respectively. These quantities correspond to concentrations of 0.98 μg $mL^{-1}$, 1.86 μg $mL^{-1}$ and 4.82 μg $mL^{-1}$, all significantly above the MIC of rifampicin for *S. aureus* (0.05 μg $mL^{-1}$). However, they are lower than the MICs of *E. coli* and *P. aeruginosa* (25 μg $mL^{-1}$ and 50 μg $mL^{-1}$), indicating that the technology against these two strains might not be effective. To gain more insight into the matter, an in-depth investigation of the antibacterial properties of the three formulations of rifampicin-loaded PCL/silica hybrids was performed.

### 3.4 The release of antibiotic is highly effective against common osteomyelitis strains

The antibacterial analysis of the materials was carried out in two subsequent steps. First, a agar disk diffusion assay was used to gain preliminary data on potential of each formulation. Then, CFU counting was performed to quantify the bactericidal effect.

The results of the halo test reflect the findings of the dilution assays used to determine the MICs: rifampicin was successfully released from all loaded hybrids with dose-dependent inhibition zones significantly increasing with higher rifampicin loading ($p < 0.05$). As expected from the MIC determination, inhibition areas were wider for *S. aureus* and smaller for both the tested Gram-negative strains. No halo was observed for pure PCL/silica samples (PS), confirming the lack of intrinsic antibacterial properties of the material. Against *S. aureus*, rifampicin was already effective at the lowest dosage (PSRL), resulting in an inhibition zone with a width of 9 mm. For PSRM and PSRH samples the width significantly increased to 12 and 17 mm, respectively. Less remarkable was the effect against the two Gram-negative strains, as it is often the case. This family of bacteria is in fact known for its lower susceptibility to antibiotics and other antimicrobial agents, owing to their more complex and resistant cell wall structure. Despite this, the highest dosage of rifampicin (PSRH) was proven effective against both *E. coli* (3 mm) and *P. aeruginosa* (5 mm width) without significant difference between the two results. No inhibitory effect was found around PSRL. A minor inhibition zone (~1 mm width) was instead observed around PSRM samples. This value is often indicated as the minimum threshold to validate the inhibitory effect of an antibacterial material (SNV 195920-1992).[67,68] In light of this result, it can be concluded that, while all formulations showed outstanding performance against *S. aureus*, the loading concentration of rifampicin in PSRM can be considered as the lower limit of concentration for the design of materials that target *E. coli* and *P. aeruginosa* and possibly other Gram-negative bacterial strains (Fig. 11).

The results of CFU counting confirmed and expanded the preliminary findings obtained by the agar diffusion assay (Fig. 12). In suspension, the results of the negative control were as expected, showing a growth curve typical of a healthy bacterial population: an initial lag phase in the first hours of culture, followed by exponential growth and finally by a plateau around $10^9$ CFU $mL^{-1}$ ($10^7$ on pellets).[69] Bacteria behaved similarly when cultured in contact with PS. All rifampicin-containing formulations were highly effective against *S. aureus*, showing a remarkable reduction in bacterial growth between six (for PSRL) and nine (for PSRH) orders of magnitude. The reduction in bacterial growth is consistent with both drug loading and drug release profiles, confirming that the antibacterial effect can be tailored by varying the amount of rifampicin added to the material.

Against Gram-negative bacteria the reduction of the CFUs in suspension was less remarkable, but significant, nonetheless. In particular, PSRM inhibited the growth of P. *aeruginosa* and *E. coli* of 3.0-log and 1.8-log, respectively. The inhibition then increases to more than 5-log when the two strains are put in contact with PSRH. The logarithmic reduction in bacterial growth for all formulations and strains is reported in Table 3. The antifouling properties of the materials were also tested by counting the number of bacterial cells that adhered to the pellets. Once again, the hybrids showed remarkable antifouling properties against *S. aureus*, significantly reducing the number of cells found on the samples in a dose-dependent fashion, from 2.8-log for PSRL to 6.7-log for PSRH. Bacterial growth on the pellets was also reduced in the case of *E. coli* and *P. aeruginosa*, although for these two strains the reduction was limited to 1–2 orders of magnitude and the bacteria were not susceptible to PSRL (see Fig. 12 and Table 3).

Results of the quantitative antibacterial testing confirmed the potential of rifampicin sustained release from PCL/silica

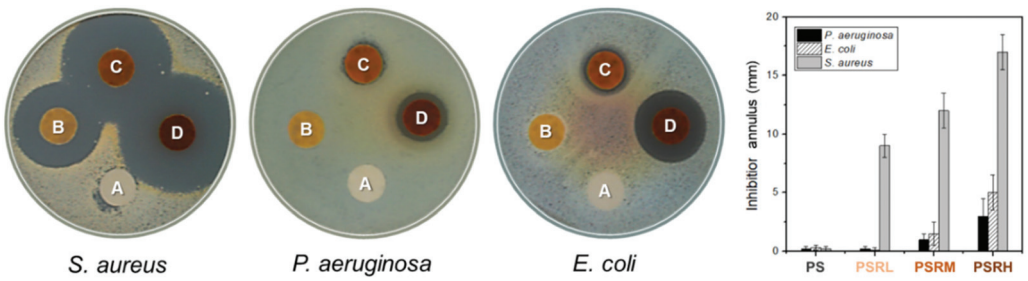


Fig. 11 Images of a typical agar diffusion assay of PS (A), PSRL (B), PSRM (C) and PSRH (D) samples against *Staphylococcus aureus*, *Pseudomonas aeruginosa* and *Escherichia coli*. On the graph on the right, a quantification of the inhibition width is reported.

 

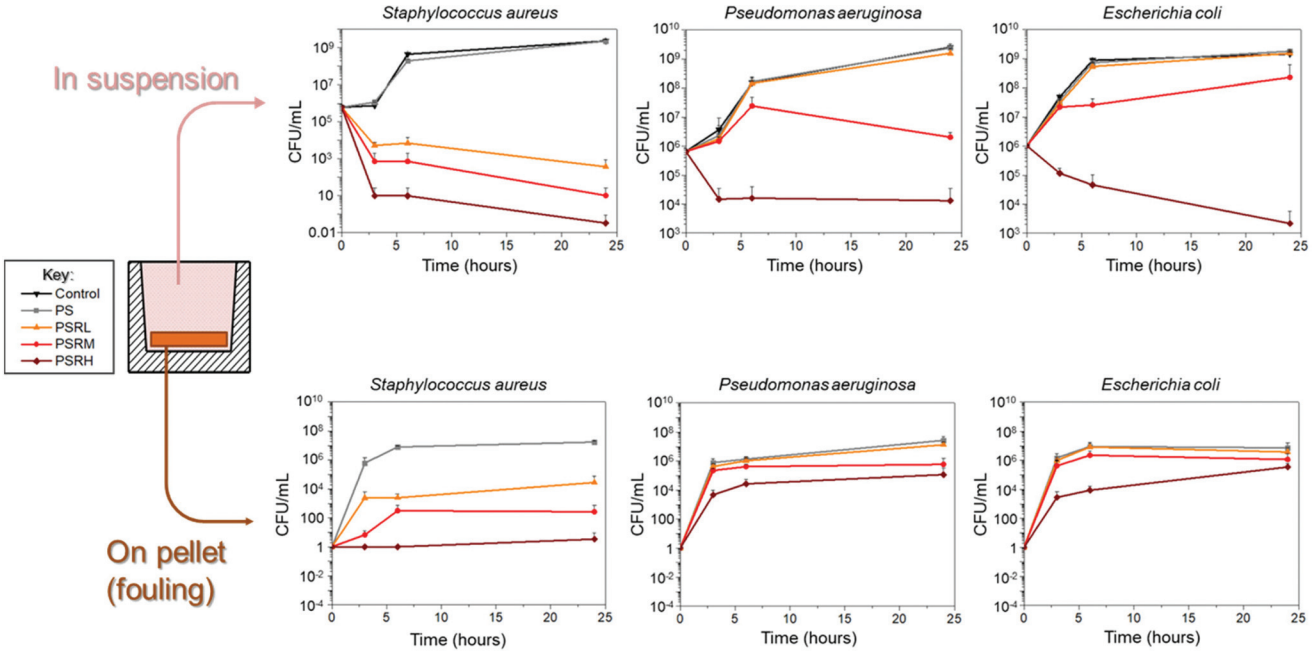


Fig. 12 Bacterial growth curves (CFU counting) for *S. aureus*, *P. aeruginosa* and *E. coli* in contact with all formulations of hybrids. Cells in suspension (top) and attached to the samples (bottom) were both counted. Empty culture wells with αMEM were used as negative control when relevant.

hybrids and helped clarify the optimal window of concentration to achieve a broader spectrum of effect against both Gram-positive and -negative bacteria. According to our data, rifampicin loading equal and superior to PSRM seems to give enough antibacterial effect to inhibit the growth of all tested strains tested. On the other hand, PSRL is a good candidate against *S. aureus*, but did not show any effect against the Gram-negative bacteria tested in this study. Considering the high density of the starting inoculum (*i.e.*, $10^6$ CFU $mL^{-1}$), this experiment was designed as a worst-case scenario. In realistic settings, the entity of bacterial contamination is several orders of magnitude smaller[70] and the performance of PSRM against all strains can be considered successful. In future work, increasing the loading of rifampicin towards the values of PSRH (*e.g.*, double it) might be a good strategy to improve the results. However, the content of rifampicin cannot be increased *ad libitum*: as observed in the rifampicin tailoring section, concentrations above 20 μg $mL^{-1}$ can lead to harmful cytotoxic effects. Therefore, it is important to characterize the effect of the hybrids on eukaryotic cells.

### 3.5 The hybrids are cytocompatible and osteogenic

Excessive release of rifampicin can have a detrimental effect on the growth and proliferation of osteoblasts and eukaryotic cells in general. For this reason, the cytocompatibility of primary rat osteoblasts (RPOs) cultured in presence of rifampicin-loaded PCL/silica hybrids was tested by a formazan-based XTT colorimetric assay. Cell viability was measured at 2 and 7 days to evaluate initial cytotoxicity and cell proliferation as a function of rifampicin content and release (see Table 1 and Fig. 10). Results for all formulations are reported in Fig. 13A. At day 2, all formulations performed similarly to the control sample (RPOs cultured on tissue culture polystyrene, TCPS), except for PSRM, where cell viability slightly increased over 100%, most probably because of a stochastic variation. It could also be due to a positive effect of silicates release from the hybrids,[71] however no such effect was observed with PS and PSRL materials. After one week of culture, cell viability measured with all formulations was comparable to that of the negative control, except for PSRH. With the high concen-

Table 3 $Log_{10}$ decrease of bacterial inhibition after 24 hours following the contact with rifampicin-loaded hybrids. The values are calculated with respect to the negative control (suspension) or to PS (pellet)

| | PSRL | | PSRM | | PSRH | |
|---|---|---|---|---|---|---|
| | suspension | pellet | suspension | pellet | suspension | pellet |
| *S. aureus* | 6.8 | 2.8 | 8.4 | 4.8 | 9.8 | 6.7 |
| *P. aeruginosa* | 0.2 | 0.3 | 3.0 | 1.7 | 5.2 | 2.4 |
| *E. coli* | 0.0 | 0.3 | 1.8 | 0.8 | 5.8 | 1.3 |

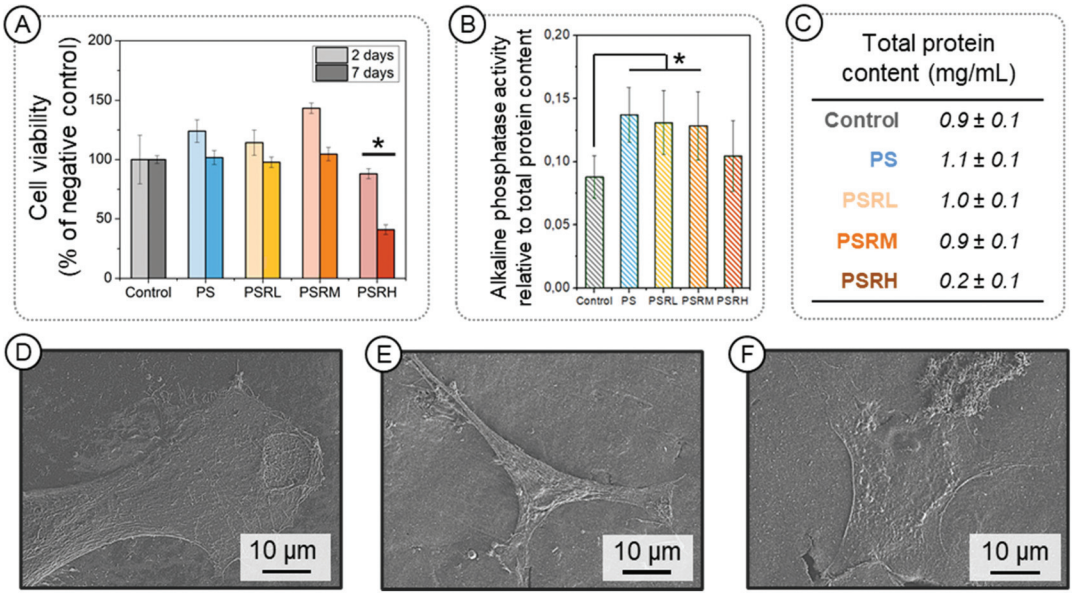


**Fig. 13** (A) Cell viability of primary rat osteoblasts (RPOs) cultured in contact with each material for 2 (left) and 7 (right) days. The cytotoxic effect of PSRH can be clearly observed at 7 days. All other formulations performed similarly to a negative control (TCPS). (B) ALP activity at 14 days plotted with respect to the (C) total protein content. Note that proteins are highly reduced in PSRH samples. SEM images showing attachment of RPOs on (D) PCL, (E) PS and (F) PSRM pellets.

trations of rifampicin released from this formulation (>100 ppm), a significant decrease in viability was observed, dropping to 41%. This result is in agreement with data from the literature.[72,73] In addition, they are consistent with our findings in terms of antibiotic release: PSRH is expected to release in αMEM a quantity of rifampicin (Fig. 10) with a detrimental effect on osteoblasts (Fig. 3).

Regarding the other formulations, rifampicin did not have measurable negative effects on cells. On the contrary, these hybrids were found to have a beneficial effect on osteoblasts, thanks to the release of silicates from the inorganic component of the material. In particular, the activity of alkaline phosphatase (ALP) was measured as a good preliminary marker to evaluate the osteostimulative potential of the hybrid materials prepared in this study. Results show that the presence of silica gel can be associated with a significant increase in ALP activity in the case of PS, PSRL and PSRM samples (Fig. 13B). The effect observed with the highest concentration (PSRH) seemed comparable to that of the negative control. However, closer examination of the result led to the identification of an artifact: the ALP activity was calculated as a relative amount, with respect to the total protein content. As shown in Fig. 13C, the protein content of RPOs cultured in contact with PSRH is remarkably lower (*circa* fourfold) than the usual quantity (around 1 mg $mL^{-1}$). The normalization, as a consequence, would indicate overexpression of the ALP activity, whereas the low protein content indicates that most cells are in fact dead.[74] These data provide a first indication of the osteostimulative effect of rifampicin-loaded hybrids, as well as on the cytotoxic effect of excessive quantities of rifampicin. However, they should be intended as a proof of concept of the technology. Further biological investigations should be carried out to corroborate the results presented here. Additional markers should be used to obtain a more comprehensive characterization of the gene and protein expression of cells (*e.g.*, collagen I, RUNX2) and mineralization (*e.g.*, alizarin red staining). Furthermore, although not performed in this study, the option of co-culturing bacteria and eukaryotic cells could be another interesting development, providing more physiological-like information into the therapeutic performance of the materials.

In parallel to metabolic and ALP activity, cell adhesion on the materials was also investigated. In light of their inferior performance, PSRL and PSRH were not considered at this step. Fig. 13D shows a typical cellular morphology on pure PCL. Although low adhesion and spherical morphology were previously reported for cells cultured on PCL[26] probably because of the hydrophobicity of the material, our results confirm PCL as a good substrate for osteoblast adhesion. RPOs are numerous and their morphology has all the evidence of healthy cells: elongated spindle shaped with several filopodia. Similar results were obtained using hybrids with or without rifampicin as substrate (Fig. 13E and F). The mild enhancement in hydrophilicity due to the presence of the inorganic phase is thought to facilitate cell adhesion.[75,76] This improvement could be further enhanced using other sol–gel formulations with apatite-forming ability (for instance adding calcium). As previously mentioned, this was not possible to date because of the chemically fragile nature of rifampicin. However, we do not exclude that this could be a promising avenue of future development to further increase the osteostimulative potential of these antibacterial hybrids.

## 4. Concluding remarks

The goal of this work was to prove the potential of PCL/silica hybrids as drug delivery carriers for the treatment of bone defects, tackling in particular the risk of bone infections (osteomyelitis). Our approach consisted in the design of a multiple delivery platform that can be antibacterial and osteostimulative at the same time, in other words with a dual therapeutic effect, and with independent release kinetics of the various therapeutic agents (*i.e.*, decoupled release). Before the development of the material, antibiotic rifampicin was selected among other candidate drugs and its effect on both eukaryotic and prokaryotic cells was characterized. This step allowed the identification of an optimal range of concentrations with sufficient antibacterial effect and negligible toxicity against osteoblasts. The findings of this first stage led to the successful fabrication of a series of formulations of PCL/silica hybrids with varying antibiotic content. These materials are characterized by adequate hydrophilicity and stability in physiological-like fluids for the selected application. Most notably, they offer a dual controlled release of rifampicin and silicates with superior pharmacokinetics compared to current commercial antibacterial bone cements (*e.g.*, gentamicin-impregnated PMMA). Spectrophotometric measurements confirmed that rifampicin can be delivered in tailorable concentrations with sustained release for several weeks. The drug delivery determines outstanding antibacterial properties, especially against *S. aureus*, the major responsible strain for osteomyelitis. Satisfactory performance was also obtained against two Gram-negative strains. At the same time, PCL/silica hybrids quickly release silicates in a physiological environment. These therapeutic ions were associated with increases in the ALP activity of primary osteoblasts compared to a negative control, indicating that they can provide significant osteostimulative effect, helping cells to proliferate and differentiate correctly. The findings of this study strongly suggest that developing PCL/silica hybrids further could lead to a biomaterial with ideal pharmacokinetics, strong bone regeneration potential and high throughput producibility. Since PCL-based hybrids are a very versatile platform, many possible developments could be envisaged in the future. Among others, two major topics should be explored to exploit the drug delivery potential of PCL-based hybrids to its full extent. First, rifampicin could be used in combination with other drugs known to have synergistic effects with it (*e.g.*, imidazole, ciprofloxacin). This strategy could simultaneously increase the efficacy of the material and reduce the risk of resistance development. Secondly, efforts should be made in order to increase the complexity of the inorganic component. Results so far were obtained with pure silica hybrids. However, the biological performance of these materials could highly benefit from the introduction of more elements. Calcium for instance could help improve apatite formation. Silver or copper could sharpen and optimize the antibacterial properties. Finding clever ways to incorporate these ions without degrading rifampicin (and/or other drugs) remains a crucial challenge.

## Conflicts of interest

The authors declare no conflict of interest.

## Acknowledgements

This project was supported by OST Laboratoires and has received funding by the EU under the European Regional Development Fund (ERDF) program ("Fonds Européen de Développement Régional" FEDER), Région Auvergne-Rhône-Alpes under the "pack Ambition Recherche" program (BIOSTEON project, grant agreement no. AV0016426), and the Agence Nationale de la Recherche of the French government through the program "Investissements d'Avenir" (16-IDEX-0001 CAP 20-25, Hub Innovergne project). The authors would like to thank Christelle Blavignac and Claire Szczepaniak at the Centre Imagerie Cellulaire Santé (Clermont-Ferrand Faculty of Medicine) for SEM imaging of cell adhesion on biomaterials, and Dr Mhammed Benbakkar at the Laboratoire Magma et Volcans (CNRS and Université Clermont Auvergne mixed unit UMR 6524) for ICP-OES measurements.

## References

1 A. Ferrando, J. Part and J. Baeza, *J. Bone Jt. Infect.*, 2017, **2**, 194.
2 F. A. Waldvogel, G. Medoff and M. N. Swartz, *N. Engl. J. Med.*, 1970, **282**, 260.
3 R. Berebichez-Fridman, P. Montero-Olvera, R. Gómez-García and E. Berebichez-Fastlicht, *Med. Hypotheses*, 2017, **105**, 63.
4 X. Zhang, Q. Lu, T. Liu, Z. Li and W. Cai, *BMC Infect. Dis.*, 2019, **19**, 823.
5 M. Dudareva, A. J. Hotchen, J. Ferguson, S. Hodgson, M. Scarborough, B. L. Atkins and M. A. McNally, *J. Infect.*, 2019, **79**, 189.
6 P. Dinh, B. Hutchinson, C. Zalavras and M. Stevanovic, *Semin. Plast. Surg.*, 2009, **23**, 108.
7 E. S. R. Darley and A. P. MacGowan, *J. Antimicrob. Chemother.*, 2004, **53**, 928.
8 L. O. Conterno and M. D. Turchi, *Cochrane Database Syst. Rev.*, 2013, CD004439.
9 B. N. Kim, E. S. Kim and M. D. Oh, *J. Antimicrob. Chemother.*, 2014, **69**, 309.
10 D. W. Haas and M. P. McAndrew, *Am. J. Med.*, 1996, **101**, 550.
11 S. C. Manolagas, *Endocr. Rev.*, 2000, **21**, 115.
12 B. Klosterhalfen, K. M. Peters, C. Töns, S. Hauptmann, C. L. Klein and C. J. Kirkpatrick, *J. Trauma: Inj., Infect., Crit. Care*, 1996, **40**, 372.
13 H. Serati-Nouri, S. Rasoulpoor, R. Pourpirali, S. Sadeghi-Soureh, N. Esmaeilizadeh, M. Dadashpour, L. Roshangar and N. Zarghami, *Life Sci.*, 2021, **285**, 119947.

14 S. G. Rotman, K. Thompson, D. W. Grijpma, R. G. Richards, T. F. Moriarty, D. Eglin and O. Guillaume, *J. Orthop. Transl.*, 2020, **21**, 136.
15 X. Xu and J. Song, *Biomater. Transl.*, 2020, **1**, 51.
16 M. S. Saveleva, A. N. Ivanov, M. O. Kurtukova, V. S. Atkin, A. G. Ivanova, G. P. Lyubun, A. V. Martyukova, E. I. Cherevko, A. K. Sargsyan, A. S. Fedonnikov, *et al.*, *Mater. Sci. Eng., C*, 2018, **85**, 57.
17 F. Sepúlveda, N. Butto, J. L. Arias, M. Yazdani-Pedram, P. K. Szewczyk, A. Gruszczynski, U. Stachewicz and A. Neira-Carrillo, *Cryst. Growth Des.*, 2020, **20**, 5610.
18 M. S. Saveleva, A. N. Ivanov, J. A. Chibrikova, A. A. Abalymov, M. A. Surmeneva, R. A. Surmenev, B. V. Parakhonskiy, M. V. Lomova, A. G. Skirtach and I. A. Norkin, *Macromol. Biosci.*, 2021, **21**, 2100266.
19 C. W. Schlickewei, S. Yarar and J. M. Rueger, *Orthop. Res. Rev.*, 2014, 71.
20 H. Lu, Y. Liu, J. Guo, H. Wu, J. Wang and G. Wu, *Int. J. Mol. Sci.*, 2016, **17**, 334.
21 J. Geurts, J. J. Chris Arts and G. H. I. M. Walenkamp, *Injury*, 2011, **42**(2), S82–S86.
22 I. Qayoom, R. Verma, P. A. Murugan, D. B. Raina, A. K. Teotia, S. Matheshwaran, N. N. Nair, M. Tägil, L. Lidgren and A. Kumar, *Sci. Rep.*, 2020, **10**, 14128.
23 C. Qin, L. Xu, J. Liao, J. Fang and Y. Hu, *BioMed Res. Int.*, 2018, **2018**, 1.
24 R. Ene, M. Nica, D. Ene, A. Cursaru and C. Cirstoiu, *EFORT Open Rev.*, 2021, **6**(5), 297–304.
25 J. Y. Ferguson, M. Dudareva, N. D. Riley, D. Stubbs, B. L. Atkins and M. A. McNally, *Bone Jt. J.*, 2014, **96B**(6), 829–836.
26 C. Bossard, H. Granel, Y. Wittrant, É. Jallot, J. Lao, C. Vial and H. Tiainen, *Biomed. Glas.*, 2018, **4**, 108.
27 H. Granel, C. Bossard, A.-M. Collignon, F. Wauquier, J. Lesieur, G. Y. Rochefort, E. Jallot, J. Lao and Y. Wittrant, *ACS Appl. Bio Mater.*, 2019, **2**(8), 3473–3483.
28 J. Jones, *Acta Biomater.*, 2013, **9**, 4457.
29 B. M. Novak, *Adv. Mater.*, 1993, **5**, 422.
30 E. C. Morais, G. G. Correa, R. Brambilla, J. H. Z. dos Santos and A. G. Fisch, *J. Sep. Sci.*, 2013, **36**, 636.
31 C. Marquès, J. Tasse, A. Pracros, V. Collin, C. Franceschi, F. Laurent, S. Chatellier and C. Forestier, *J. Med. Microbiol.*, 2015, **64**, 1021.
32 C. Marquès, C. Franceschi, V. Collin, F. Laurent, S. Chatellier and C. Forestier, *Genome Announc.*, 2016, **4**(2), e00198-16.
33 C. Marquès, V. Collin, C. Franceschi, N. Charbonnel, S. Chatellier and C. Forestier, *J. Antibiot.*, 2020, **73**, 91.
34 H. Ishida, C. G. Bellows, J. E. Aubin and J. N. Heersche, *Endocrinology*, 1993, **132**, 61.
35 M. I. Walash, F. Belal, M. E. Metwally and M. M. Hefnawy, *Anal. Lett.*, 1993, **26**, 1905.
36 P. Dworsky and M. Schaechter, *J. Bacteriol.*, 1973, **116**, 1364.
37 M. T. Heinrichs, R. J. May, F. Heider, T. Reimers, S. K. B. Sy, C. A. Peloquin and H. Derendorf, *Int. J. Mycobact.*, 2018, **7**, 156.
38 B. Yang, Z. Lei, Y. Zhao, S. Ahmed, C. Wang, S. Zhang, S. Fu, J. Cao and Y. Qiu, *Front. Microbiol.*, 2017, **8**, 2125.
39 G. Li, J. Zhang, Q. Guo, Y. Jiang, J. Wei, L. L. Zhao, X. Zhao, J. Lu and K. Wan, *PLoS One*, 2015, **10**(2), e0119013.
40 Z. Breijyeh, B. Jubeh and R. Karaman, *Molecules*, 2020, **25**, 1340.
41 W. D. Winters, A. L. Tuan and D. L. Morton, *Cancer Res.*, 1974, **34**, 3173.
42 M. Singh, P. Sasi, G. Rai, V. H. Gupta, D. Amarapurkar and P. P. Wangikar, *Med. Chem. Res.*, 2011, **20**, 1611.
43 C. Bossard, H. Granel, É. Jallot, V. Montouillout, F. Fayon, J. Soulié, C. Drouet, Y. Wittrant and J. Lao, *ACS Biomater. Sci. Eng.*, 2019, **5**, 5906.
44 S. Kumar, S. Bose and K. Chatterjee, *RSC Adv.*, 2014, **4**, 19086.
45 W. Jiang, J. Shi, W. Li and K. Sun, *Polym. Eng. Sci.*, 2012, **52**, 2396.
46 D. P. Dowling, I. S. Miller, M. Ardhaoui and W. M. Gallagher, *J. Biomater. Appl.*, 2011, **26**, 327.
47 K. J. Williams and L. J. V. Piddock, *J. Antimicrob. Chemother.*, 1998, **42**, 597.
48 G. L. Siparsky, K. J. Voorhees and F. Miao, *J. Environ. Polym. Degrad.*, 1998, **6**, 31.
49 F. E. Ciraldo, E. Boccardi, V. Melli, F. Westhauser and A. R. Boccaccini, *Acta Biomater.*, 2018, **75**, 3.
50 H. Granel, C. Bossard, L. Nucke, F. Wauquier, G. Y. Rochefort, J. Guicheux, E. Jallot, J. Lao and Y. Wittrant, *Adv. Healthcare Mater.*, 2019, **8**, 1801542.
51 T. Elzein, M. Nasser-Eddine, C. Delaite, S. Bistac and P. Dumas, *J. Colloid Interface Sci.*, 2004, **273**, 381.
52 L. Liverani and A. Boccaccini, *Nanomaterials*, 2016, **6**, 75.
53 K. Phillipson, J. N. Hay and M. J. Jenkins, *Thermochim. Acta*, 2014, **595**, 74.
54 S. R. Darmakkolla, H. Tran, A. Gupta and S. B. Rananavare, *RSC Adv.*, 2016, **6**, 93219.
55 P. Innocenzi, *J. Non-Cryst. Solids*, 2003, **316**, 309.
56 R. M. Almeida and A. C. Marques, *Handb. Sol-Gel Sci. Technol.*, Springer International Publishing, Cham, 2016, pp. 1–31.
57 E. Tranquillo, F. Barrino, G. Dal Poggetto and I. Blanco, *Materials*, 2019, **12**, 155.
58 B. A. Allo, A. S. Rizkalla and K. Mequanint, *Langmuir*, 2010, **26**, 18340.
59 J. R. Jones, *Acta Biomater.*, 2013, **9**, 4457.
60 O. Ivashchenko, T. Tomila, N. Ulyanchich, T. Yarmola and I. Uvarova, *Adv. Sci., Eng. Med.*, 2014, **6**, 193.
61 F. E. Ciraldo, L. Liverani, L. Gritsch, W. H. Goldmann and A. R. Boccaccini, *Materials*, 2018, **11**, 692.
62 D. Arcos and M. Vallet-Regí, *Acta Biomater.*, 2010, **6**, 2874.
63 E. J. Kim, S. Y. Bu, M. K. Sung and M. K. Choi, *Biol. Trace Elem. Res.*, 2013, **152**, 105.
64 A. C. Kassab, K. Xu, E. B. Denkbas, Y. Dou, S. Zhao and E. Piskin, *J. Biomater. Sci., Polym. Ed.*, 1997, **8**, 947.
65 M. W. Salim, K. Shabbir, F. Ud-Din, A. M. Yousaf, H.-G. Choi and G. M. Khan, *J. Drug Delivery Sci. Technol.*, 2020, **60**, 101996.

 

66 M. Dadkhah, L. Pontiroli, S. Fiorilli, A. Manca, F. Tallia, I. Tcacencu and C. Vitale-Brovarone, *J. Mater. Chem. B*, 2017, **5**, 102.
67 M. Pollini, F. Paladini, M. Catalano, A. Taurino, A. Licciulli, A. Maffezzoli and A. Sannino, *J. Mater. Sci.: Mater. Med.*, 2011, **22**(9), 2005–2012.
68 M. J. Sánchez, J. E. Mauricio, A. R. Paredes, P. Gamero and D. Cortés, *Mater. Lett.*, 2017, **191**, 65–68.
69 M. T. Madigan, K. S. Bender, J. M. Martinko, D. H. Buckley and D. A. Stahl, *Brock Biology of Microorganisms*, 2014.
70 D. K. Ahn, H. S. Park, T. W. Kim, J. H. Yang, K. H. Boo, I. J. Kim and H. J. Lee, *Asian Spine J.*, 2013, **7**, 8.
71 T. N. Perkins, A. Shukla, P. M. Peeters, J. L. Steinbacher, C. C. Landry, S. A. Lathrop, C. Steele, N. L. Reynaert, E. F. Wouters and B. T. Mossman, *Part. Fibre Toxicol.*, 2012, **9**, 6.
72 A. Olufunsho and A. Alade, *Niger. J. Health Biomed. Sci.*, 2010, **9**(2), DOI: 10.4314/njhbs.v9i2.62590.
73 P. Saravanan, V. N. A. Dusthackeer, R. S. Rajmani, B. Mahizhaveni, C. R. Nirmal, S. E. Rajadas, N. Bhardwaj, C. Ponnuraja, A. Bhaskar, A. K. Hemanthkumar, *et al.*, *Sci. Rep.*, 2021, **11**, 1029.
74 L. S. Minamide and J. R. Bamburg, *Anal. Biochem.*, 1990, **190**, 66.
75 J. Wei, T. Igarashi, N. Okumori, T. Igarashi, T. Maetani, B. Liu and M. Yoshinari, *Biomed. Mater.*, 2009, **4**(4), 045002.
76 T. Kaur, S. Kulanthaivel, A. Thirugnanam, I. Banerjee and K. Pramanik, *Biomed. Mater.*, 2017, **12**(2), 025012.